# Effect of Relative Strength of Two Networks on Internal Fracture Process of Double Network Hydrogels as Revealed by in situ Small-Angle X-ray Scattering

Kazuki Fukao[1], Tasuku Nakajima[2,3,4], Takayuki Nonoyama[2,3], Takayuki Kurokawa[2,3], Takahiko Kawai[5]* and Jian Ping Gong[2,3,4]*

[1] Graduate School of Life Science, Hokkaido University, Sapporo, 060-0810, Japan

[2] Faculty of Advanced Life Science, Hokkaido University, Sapporo, 060-0810, Japan

[3] Global Station for Soft Matter, Global Institution for Collaborative Research and Education (GI-CoRE), Hokkaido University, Sapporo, 001-0021, Japan

[4] Institute for Chemical Reaction Design and Discovery (WPI-ICReDD), Hokkaido University, Sapporo, 001-0021, Japan

[5] Graduate School of Engineering, Gunma University, Ota, 373-0057, Japan

Corresponding to kawaitakahiko@gunma-u.ac.jp (T. Kawai) and gong@sci.hokudai.ac.jp (J. P. Gong)

**Abstract**

Double network hydrogels (DN gels) exhibit extraordinarily high strength and toughness by interplay of the two contrasting networks: the rigid, brittle network serves as a sacrificial bond that fractures at a relatively low strain, while the soft, stretchable network serves as hidden length that sustains stress by large extension afterwards. The internal fracture process of the brittle network strongly depends on the relative strength of the two networks. In this study, we study the internal fracturing process of typical DN gels that show yielding or necking under uniaxial stretching, using *in situ* small-angle X-ray scattering. Two samples consisting of the same brittle first network from poly(2-acrylamido-2-methylpropanesulfonic acid) but stretchable second network from poly(N,N-dimethylacrylamide) of different concentrations were adopted. We found that (1) the brittle network shows non-affine deformation even far below the yield strain by local fracture; (2) for the sample of low second network concentration, significant strain amplification occurs around the submicron-scale voids (defects) preexisting in the brittle network, which induces the fracture percolation of brittle network from voids to show the necking phenomenon; (3) the strain amplification at voids is suppressed in the sample of high second network concentration, and fracture of brittle network occurs dispersedly, showing yielding without necking.

**Keywords**

double network hydrogel, small-angle X-ray scattering, necking behavior, stress concentration

**TOC**

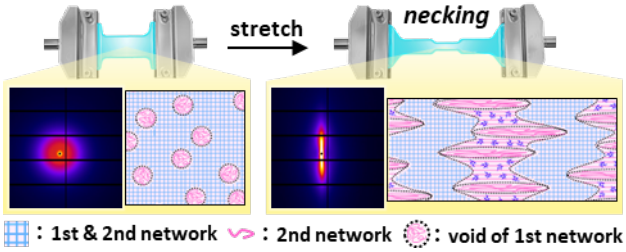

## Introduction

The double network (DN) strategy has attracted significant attention as a method for developing strong and tough polymer materials including hydrogels[1–4] and elastomers[5,6]. A typical DN material has an interpenetrated network structure consisting of two contrasting networks: one is hard and brittle, rupturing at small strain and relatively low stress; and the other is soft and stretchable, rupturing at significantly high strain and relatively high stress to the brittle one. Such contrasting DN structures were initially formed by a two-step synthesis process, in which a densely cross-linked polyelectrolyte was synthesized first as the brittle first network and then a sparsely cross-linked neutral polymer was synthesized as the stretchable second network in the presence of the brittle network.[1,2] Later on, diverse approaches were developed to synthesize the contrasting DN or triple network (TN) structures.[5–12] These approaches substantially increased the pathways to have high strength and toughness soft materials from various polymers for various applications, including artificial cartilages.[13–17]

The excellent mechanical properties of DN materials are explained with the sacrificial bond principle originating from the contrasting network structures.[2,18,19] When tensile force is applied to a DN material, the brittle network strands are preferentially broken in a wide range by scission of covalent bonds as sacrificial bonds; Owing to the soft and stretchable network, the material maintains unity, thereby

preventing the macroscopic failure. The internal fracturing of the brittle network dissipates significant amounts of energy, resulting in high toughness of the DN material.[20–22] Because of this preferential internal fracturing of the brittle network, tough DN materials usually show a yielding behavior upon uniaxial deformation. In particular, a distinct necking phenomenon often appears concomitant with this yielding behavior.[23,24] Since the necked zone is significantly softer than the unnecked zone, the brittle network in the necked zone is considered breaks into discontinuous structure.[2,19,25]

The above internal fracturing mechanism of DN materials has been proposed based on irreversible mechanical hysteresis[20], anisotropic re-swelling after stretching[19], electrostatic potential distribution[26], and chemical detection of bond breaking[5,15]. However, the microscale and nanoscale structure evolutions during the internal fracturing process are still poorly known. Direct structure observations during deformation are therefore required to elucidate the fracture process in DN materials.

Scattering is an effective method to determine microstructures of materials, including of soft materials.[27,28] Some researchers have performed scattering measurements on conventional DN hydrogels from poly(2-acrylamido-2-methylpropanesulfonic acid) (PAMPS) as the brittle first network and poly(acrylamide) (PAAm) as the stretchable second network.[29–34] Dynamic light scattering (DLS) on the undeformed DN gels showed the slow relaxation mode in addition to typical fast relaxation mode from

the network, which implies existence of submicron-scale voids in the first network synthesized from free-radical polymerization.[29,35] Small-angle neutron scattering (SANS) also revealed a strong heterogeneity of the first network at the submicron scale, thereby implying the existence of voids.[32,34] These preexisting voids, formed during the assembling of micro gels in the first network formation, are expected to remarkably affect the mechanical behavior (in particular, necking) of DN gels, as suggested by the behaviors of DN gels containing controlled void sizes and density in the first network.[36] However, the relationship between these estimated structures and the internal fracturing process as well as the yielding of the DN materials is still not known clearly. Although *in situ* SANS study on DN and TN elastomers in the pre-yielding regions has been reported recently, the results could hardly apply to the DN hydrogels that have quite different microstructure of the networks.[37]

In this study, we performed *in situ* small-angle X-ray scattering (SAXS) on DN gels at various stretch ratios up to the post-yielding region. DN gels from PAMPS as the brittle first network and poly(*N*,*N*-dimethylacrylamide) (PDMAAm) as the stretchable second network were used. We focus on how the relative strength of the two networks influences the internal fracturing process and necking phenomenon in DN material. For this purpose, we adopted two samples with the same first network formulation but different second network concentrations. The deformation of the nano-scale mesh and

submicron-scale void in the first PAMPS network is extracted from SAXS results. The birefringence measurement was also performed to characterize the deformation of the dense second PDMAAm network. The observed results should help to understand the behavior of DN materials even without the void structure.

## Experimental section

***Materials.*** 2-acrylamido-2-methylpropanesulfonic acid (AMPS) was procured from Toagosei Co. Ltd., Japan. *N*,*N*-dimethylacrylamide (DMAAm), *N*,*N'*-methylenebisacrylamide (MBAA), and 2-oxoglutaric acid (α-keto) were purchased from FUJIFILM Wako Pure Chemical Corporation, Inc., Japan. All the chemicals, except DMAAm, were used without further purification. DMAAm was used after vacuum distillation.

***Preparation of single network (SN) and double network (DN) hydrogels.*** PAMPS/PDMAAm DN gels were synthesized as previously reported.[38] PAMPS gels were synthesized by free-radical polymerization from aqueous solutions containing 1 M AMPS as a monomer, 2 mol% (to monomer) MBAA as a cross-linker, and 1 mol% (to monomer) 2-oxoglutaric acid (α-keto) as an initiator. The PAMPS hydrogels were then immersed in an aqueous solution containing 2 or 4 M DMAAm, 0.02 mol% MBAA,

and 0.01 mol% $\alpha$-keto for 1 day until reaching the swelling equilibrium. The PAMPS network remarkably swelled in the DMAAm solution, and the volume swelling ratio of PAMPS gel in DMAAm solution relative to its as-prepared state was 32.77 and 28.09 for 2 M and 4 M DMAAm, respectively. The PDMAAm network was then synthesized by irradiating PAMPS gels to obtain the PAMPS/PDMAAm DN gels. The samples prepared from 2 M and 4 M DMAAm were coded as DN-2 and DN-4, respectively. Before measurement, the DN gels were immersed in distilled water for 1 week to remove any unreacted chemicals, and the distilled water was replaced twice daily. The DN gels further swelled in water, and the volume swelling ratios of DN gels relative to the as-prepared DN gels were 2.17 and 3.74 for DN-2 and DN-4, respectively. As a result, the PAMPS network was highly pre-stretched in the DN gels, having linear pre-stretch ratios in relative to its as-prepared state $\lambda_s$ =$(32.77*2.17)^{1/3}$=4.14 and $(28.09* 3.74)^{1/3}$=4.72, for DN-2 and DN-4, respectively. The monomer molar ratios of the second network to the first network were 65.54 and 112.38 for DN-2 and DN-4 samples, respectively. The volume changes of the first and second networks of DN gels are summarized in Supporting Information, **Table S1**. For references, PAMPS first single network (SN) gels was also prepared from an aqueous solution containing 1 M AMPS, 2 mol% MBAA, and 1 mol% α-keto, and the PDMAAm second SN hydrogels, denoted as SN-2 and SN-4, were prepared from an aqueous solution containing 2 or 4 M DMAAm, 0.02 mol% MBAA, and 0.01 mol% $\alpha$-

keto, respectively. The volume swelling ratios of SN-2 and SN-4 in swollen state relative to their as-prepared state were 2.01 and 4.38, respectively.

***Tensile measurement.*** Uniaxial tensile test was performed to evaluate the mechanical properties of the obtained DN gels and its corresponding second SN gels. First, samples were cut into dumbbell shapes (15 mm gauge length and 10 mm width). Then, uniaxial tensile test was performed at a constant velocity of 100 mm/min by using a commercial tensile tester (Instron 5965, Instron Co., USA).

***Birefringence measurement.*** To clarify the orientation of concentrated second PDMAAm network in the gels under uniaxial stretching, quantitative evaluation of birefringence was performed by a polarized optical microscope (Eclipse LV100N POL, Nikon Co., Japan) and the Berek compensator (Nichika Inc., Japan). Birefringence, $\Delta n$, was obtained by dividing the retardation value, $R$, by the sample thickness, $d$ (i.e., $\Delta n = R/d$). The thickness $d$ at each stretch ratio $\lambda$ was measured by a thickness meter. To compare birefringence between samples with different second network concentrations, the normalized birefringence obtained by dividing $\Delta n$ with the second monomer concentration was adopted.

***SAXS measurement.*** *In situ* SAXS measurements during stretching of the gels were performed at BL05XU of SPring-8 (Hyogo, Japan). The extremely high brightness of the undulator beamline permits fast data collection before causing distinct drying of hydrogels in air. The wavelength of the incident X-

ray was 1 Å (12.4 keV in energy), and the sample-to-detector distance was 4 m. The gels of dumbbell shape (15 mm gauge length and 10 mm width) were set to the in-line tensile tester and were uniaxially stretched step-wise in the horizontal direction at a velocity of 2 mm/s from deformation ratio $\lambda$ = 1 to fracture, with step width $\Delta\lambda$ = 0.5 for 1 < $\lambda$ < 2 and $\Delta\lambda$ = 0.25 for $\lambda$ > 2. The exposure time of the sample to X-ray beam was 10 s for each $\lambda$. The scattering patterns were obtained via 2D detector PILATUS3 S 1M (Dectris Ltd., Switzerland). The beam position on the gels was slightly changed at each $\lambda$ to avoid any significant damage to the gels due to the X-ray exposure. Each experiment was performed at least on 3 samples to minimize the error.

The 2D scattering images were treated with background subtraction and normalization as follows. First, the transmittance of samples, $T_s$, to the X-ray beam was calculated from the incident beam intensity measured by the ionization chamber (IC) at sample stage $IC_0$ and the transmitted beam intensity was measured by a PIN diode embedded in the beam stopper $IC_1$.

$$T_s = \frac{(\mathrm{IC}_1^s - \mathrm{IC}_1^d)}{(\mathrm{IC}_1^a - \mathrm{IC}_1^d)} \Big/ \frac{(\mathrm{IC}_0^s - \mathrm{IC}_0^d)}{(\mathrm{IC}_0^a - \mathrm{IC}_0^d)} \qquad (1)$$

where superscripts *s*, *a*, and *d* stand for the beam intensities of the sample, air, and dark, respectively. Then, the scattering intensities of samples after thickness correction, $I_{corr}$, were obtained by image calculator processing on Image J (v1.49) software.

$$I_{corr} = \left(\frac{I_S}{T_s} - I_a\right) \times t_c \quad (2)$$

where $I_s$ is the scattering image of the sample, $I_a$ is air scattering image, and $t_c$ is the thickness correction factor determined from the Lambert–Beer law using transmittance $T_s$ at undeformed ($\lambda = 1$) and deformed ($\lambda$) states of the sample assuming that the density is constant under deformation.

$$t_c = \frac{\ln T_{s,\lambda=1}}{\ln T_{s,\lambda}} \quad (3)$$

The corrected 2D scattering images were converted into 1D intensity profiles by integrating the scattering intensity in the azimuth direction against the scattering vector $q$, defined as

$$q = \frac{4\pi}{\lambda} \sin\frac{\theta}{2} \quad (4)$$

where $\theta$ is the scattering angle calibrated by the diffraction pattern of dried collagen. The 1D intensity profiles for the directions perpendicular and parallel to stretching were obtained by integrating over azimuthal angles in the range of 90°±20° and 0°±20°, respectively.

## Results and Discussion

### *Uniaxial tensile test and birefringence*

**Fig.1 (a)** shows the tensile behaviors of the two DN gels synthesized from the same first network but with two different second monomer concentrations. Their stress ($\sigma$)-stretching ratio ($\lambda$) curves overlap

at low $\lambda$, and both of them show yielding behavior. However, their $\sigma$-$\lambda$ curves deviate from each other at large $\lambda$ (>2), showing significantly different yielding behaviors. For the DN-2 gel with low second monomer concentration, a clear stress peak appeared at the yield point and the necking phenomenon was observed after yielding (**Fig.1 (b-i)**). The stress in the DN-4 gel with high second monomer concentration saturated at the yielding point, and the sample deformed homogeneously without showing the necking behavior (**Fig.1 (b-ii)**). These results clearly indicate that the yielding and necking behaviors of DN gels depend on the second network concentration that changes the mechanical balance between the two networks, although the second network alone is much softer than the DN gels, as seen in **Fig.1 (a)**.

When the internal rupture in the first network occurs in DN gels, the load carried by these broken strands is partly transferred to the second network, inducing microscopic stretching and orientation of the second network along the tensile direction. This effect can be observed from the change in the birefringence of the DN gels during stretching, because the second monomer molar concentration in the DN gel is more than 60 times higher than in the first network. **Fig.1(c)** shows the normalized birefringence for the two DN samples and their corresponding second SN gels. For the same second network concentration, the birefringence of the DN samples is slightly stronger than their corresponding SN gels at small $\lambda$ ($1<\lambda<3$), and gradually increases with $\lambda$. However, birefringence of the DN samples becomes

distinctly stronger than their corresponding SN gels when λ is beyond the yielding point (λ>3). In particular, the birefringence of DN-2 in the necking region rapidly increases above the yielding point and becomes significantly higher than its corresponding SN, indicating significant local orientation of the second network in the necking region. On the other hand, the birefringence of DN-4 that shows homogeneous deformation gradually increases even above the yielding point, showing a modest increase than its corresponding SN gel above the yielding point. These results again confirm the strong local orientation of the second network in DN-2 but not in DN-4 by yielding. The stronger birefringence of DN-4 (or SN-4) than DN-2 (or SN-2) even after normalization by the second network concentration should be attributed to the enhanced entanglement of the sample prepared at the higher concentration. These mechanical and optical results suggest different fracturing processes and structure evolutions for the two DN gels under uniaxial extension. Above the yielding point, the first network of the DN-2 sample, which shows necking, breaks into discontinuous structure and the load between the discontinuous regions is carried by the second network, which induces local strain amplification and strong orientation of the second network. In contrast, the first network of the DN-4 sample still has a continuous structure above the yielding, without local strain amplification and strong second network orientation.

1

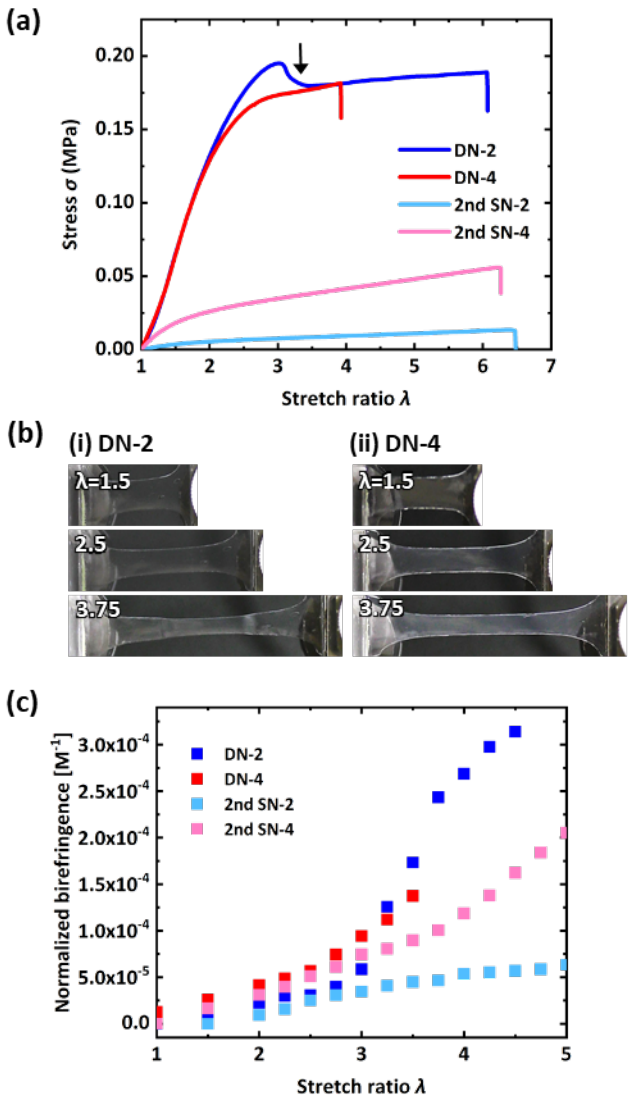


Fig.1 (a) Uniaxial tensile stress-stretch ratio curves of the DN gels with different second monomer concentration and its corresponding 2nd SN gels. The arrow indicates starting point of necking. (b) The optical images of (i) DN-2 and (ii) DN-4 gels under uniaxial stretching. (c) Normalized birefringence of DN-2, DN-4 and its corresponding 2nd SN gels under uniaxial stretching. The 2nd SN gels were used at as-prepared state.

***SAXS measurement***

SAXS results for the undeformed first SN, second SN, and DN gels in swollen state are shown in **Fig.2(a-b)**, where DN-2 and its corresponding SN were used as typical examples. Isotropic scattering images are observed in all cases (**Fig.2(a)**). The 1D scattering profiles can be divided into high-$q$ and low-$q$ regions (**Fig.2(b)**). In the high-$q$ region (typically $0.2 < q < 1$), the profiles of the DN gels obey the Ornstein–Zernike (OZ)-type scattering behavior:

$$I(q) = \frac{I_0}{1+\xi^2 q^2} \qquad (5)$$

where $I_0$, $\xi$, and $q$ are the forward scattering intensity, correlation length, and scattering vector, respectively. The OZ-type scattering behavior, originating from the concentration fluctuation of the polymer strands, is typically found in the scattering profile of polymer solutions and gels.[39–42] The correlation length, $\xi$, is related to the shoulder position in the 1D scattering profiles; the shoulder at lower $q$ means larger $\xi$. Comparing the scattering profiles of SNs, we found that the shoulder of the second SN profile is located toward lower $q$ than the first SN profile, which relates to larger $\xi$ of the second SN than that of the first SN. In addition, a small peak (so called polyelectrolyte peak) was found in the first SN profile owing to the polyelectrolyte nature of the first network.[32,43,44] For the SAXS profile of the DN gel, scattering should originate from the second network, because the concentration of the second network was much higher

than that of the first network in the DN gels. However, the scattering vector $q$ at the shoulder position in the 1D profiles of the DN gel is much closer to that of the first network than that of the second network. This suggests that the concentration fluctuation of the second network, which corresponds to the correlation length of the DN gels, is controlled by the mesh of the rigid first network as a skeleton through strong entanglement between the first and second networks. A similar hypothesis has also been indicated based on the DLS measurement.[30] To confirm this hypothesis, we performed SAXS measurements on the DN-2 gels having varied first network cross-linking densities (Supporting Information, **Figure S1**). Although the second network composition of these DN gels is the same, the shoulder position in the scattering profiles shifts to higher $q$ when the first network cross-linking density increases, indicating that the first network mesh size becomes smaller with an increase in the cross-linking density. Furthermore, the correlation lengths $\xi$ of the DN gels calculated from the scattering profiles using OZ-type function well agreed with the mesh sizes of their corresponding single first network obtained from the mechanical measurements (**Figure S1**). Based on these investigations, we conclude that the OZ-type scattering profiles of the DN gels in the high-$q$ region reflect the nanometer-scale mesh structure of their first network.

In the low-$q$ region (typically $0.035 < q < 0.2$), large anomalous scattering appears on the scattering profile of the gels, which indicates the existence of a large-scale structure. In particular, most

significant anomalous scattering was observed on the SAXS profile of the DN gel, suggesting an enhancement of the large-scale inhomogeneity in the second network by forming the double network structure. We believe that the enhanced inhomogeneity in the second network of the DN gel originates from preexisting voids of the first network in the DN gel. The previous DLS studies on DN gels suggested submicrometer-scale voids in the first network of the DN gels, and the second network in the voids showed slower cooperative diffusion than the second network in the mesh of the first network.[29,35] It is consistent with the assumption that the void region has a lower shear modulus than that of the non-void region. This is because the cooperative diffusion coefficient is positively related to shear modulus $\mu$ and bulk modulus $K$ of the gel. Shear modulus $\mu$, which depends on the cross-linking density, should be significantly higher in the mesh region than in the void region because of the strong entanglement of the second network to the first network. Based on these investigations, we conclude that the anomalous scattering of DN gels in the low-$q$ region reflects the submicrometer-scale void structure of their first network (**Fig.2(c)**).

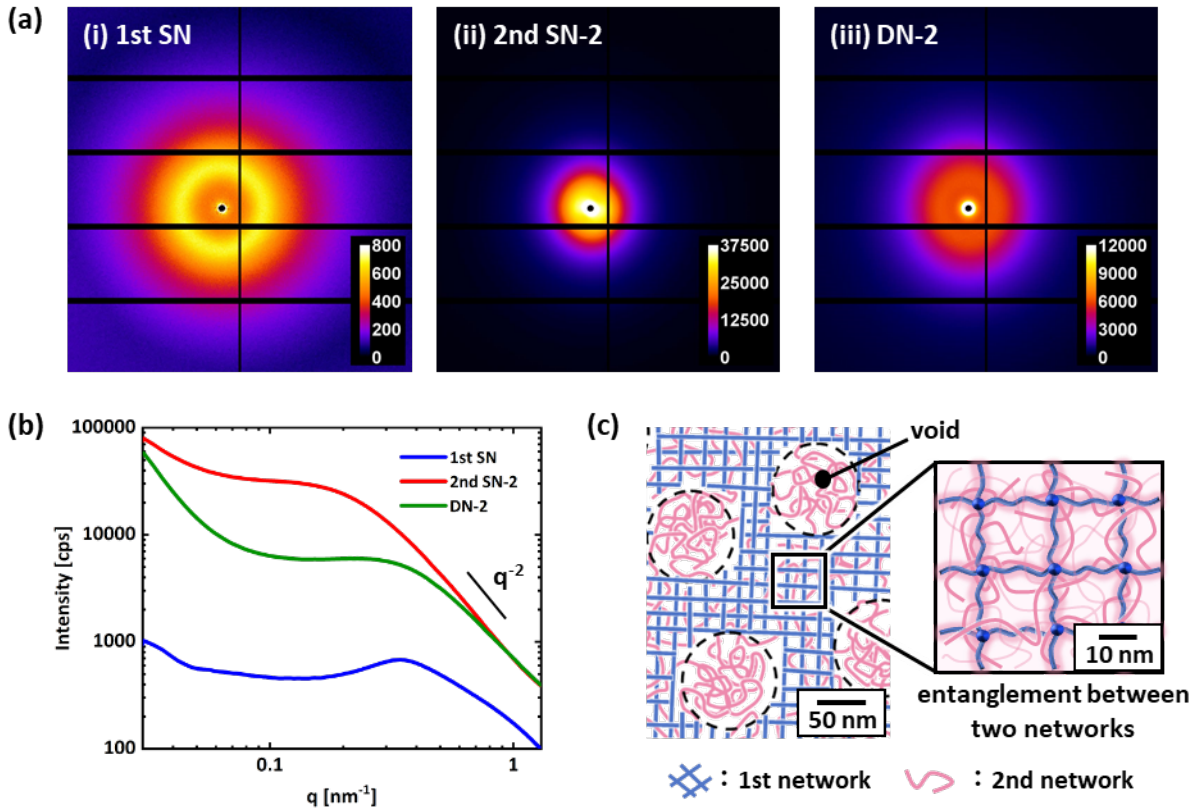


Fig.2 (a) 2-dimensional SAXS images of (i) 1st PAMPS SN gel, (ii) 2nd PDMAAm SN-2 gel, and (iii) DN-2 gel at their undeformed state. (b) 1-dimensional SAXS profiles of these gels obtained from the 2D images. (c) Schematic illustration of a DN gel containing voids in the first network. The second network strongly entangles with the first network.

The above discussion suggests that one can extract nanometer- and submicrometer-scale structural information of the first network from the SAXS profiles of the DN gels. Subsequently, *in situ* SAXS measurements on the uniaxially deformed DN-2 gel was performed to investigate the stretching-induced structural changes in the two different scales. The 2D SAXS images of the DN-2 gel at different stretching ratios are shown in **Fig.3(i)**. After observing the necking phenomenon, the X-ray was exposed on the necking region. The scattering patterns of the DN gels changed from isotropic to streak with an increase in stretch ratio $\lambda$. This pattern transition to the streak indicates a change in the submicrometer-scale void structure from the isotropic shape to anisotropic ellipsoidal shape on stretching. To investigate the changes in the mesh size in the directions parallel and perpendicular to the stretching direction, 1D profiles in the directions parallel and perpendicular to the tensile deformation were obtained by angle-selective integration. As seen in **Fig. 3(i),** in the high-$q$ region, the scattering profiles relating to the nanometer-scale mesh size of the first network still obey the OZ-type pattern regardless of the stretch ratio, thereby suggesting that the first network mesh structure is hardly changed in the deformed DN-2 gels. However, the shoulder in the scattering profile of the deformed DN gels slightly shifts with an increase in stretch ratio $\lambda$. The shoulder in the parallel profiles shifts to lower $q$, whereas that in the perpendicular profiles shifts to higher $q$ with the stretching ratio. These results are qualitatively consistent with the

common behavior that the mesh of the (first) network is elongated parallelly but compressed perpendicularly to the direction of stretching. The DN-4 gel also shows a streak pattern at large deformation and the shifts of the shoulders towards opposite *q* directions in the parallel and perpendicular 1D profiles (**Fig. 3(ii)**).

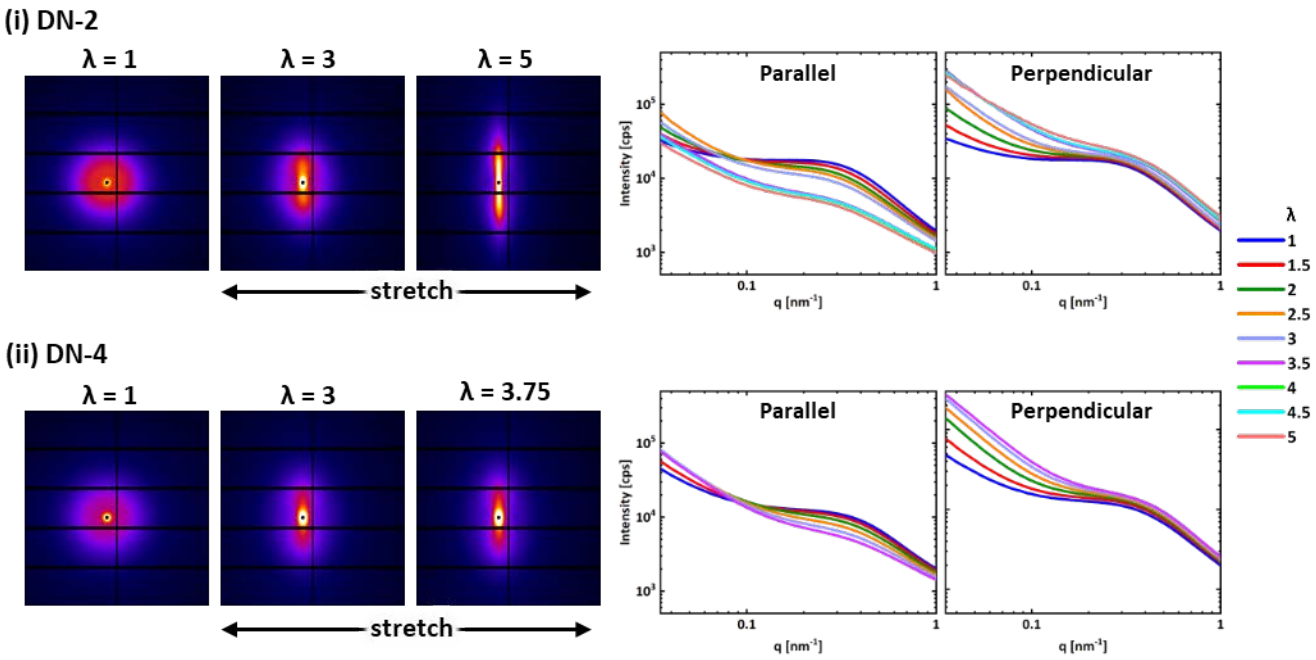


Fig.3 Representative 2D SAXS images and 1D SAXS profiles of the (i) DN-2 and (ii) DN-4 samples under uniaxial stretching. 1D profiles were obtained from parallel and perpendicular directions in relative to the tensile deformation. Above the yielding point, the results of DN-2 are for their necking region.

Focusing on these changes in the scattering data of DN gels, we quantitatively evaluated the structural change in the DN gels upon uniaxial deformation in different size scales using two types of analysis methods. First, we analyzed the submicrometer-scale void structure using the Ruland streak method. This method has been widely used to analyze oblong structures such as shish and void lengths.[45–48] For azimuthal distributions of the streak that obey the Lorentz function, the average void length $\langle L_{void} \rangle$ and azimuthal width owing to misorientation of voids $B_\varphi$ are described by the following equation using the Ruland method:

$$qB_{obs} = \frac{2\pi}{\langle L_{void} \rangle} + qB_{\varphi} \quad (6)$$

where $B_{obs}$ represents the radian of full width at half maximum in the azimuth direction of the streak at scattering vector $q$. From equation 6, the $qB_{obs}$ versus $q$ plot shows a linear line, and $\langle L_{void} \rangle$ and $B_\varphi$ can be obtained from the intercept ($=2\pi/\langle L_{void} \rangle$) and slope of the linear line, respectively. Furthermore, the orientation degree of voids, $f_{void}$, can be calculated from

$$f_{void} = \frac{180 - B_{\varphi}}{180} \quad (7)$$

We have confirmed that the Lorentz function fits well the azimuthal distributions of streak peaks of DN gels in the range of 70°–110°, and the $qB_{obs}$ versus $q$ plots at various stretching ratios $\lambda$ shows a good linearity in the low-$q$ region (**Supporting Information, Fig.S2**). Therefore, we applied the Ruland

method to analyze our streak patterns.

The dependence of the void length along the stretch direction, $<L_{void}>$, of DN gels on stretching ratio, $\lambda$, is shown in **Fig.4(a)**. For DN-2, $<L_{void}>$ first increased gradually with $\lambda$ then increased rapidly near the necking point. After reaching the necking point, $<L_{void}>$ decreased and became constant during necking propagation. In contrast, the $<L_{void}>$ of the DN-4 gel increased only weakly with $\lambda$ until the sample fractured, without showing any significant increase near the yielding point. The dependence of the orientation degree of voids, $f_{void}$, on stretching ratio $\lambda$ is shown in **Fig.4(b)**. The $f_{void}$ of DN-2 also showed a rapid increase near the necking point and became constant during necking propagation; whereas $f_{void}$ of the DN-4 gel increased linearly with the global deformation until the sample failure.

To compare the macro-scale deformation with micro-scale deformation, the void deformation ratio along the stretch direction, $\lambda_{void}$, was evaluated based on $\langle L_{void} \rangle$ at $\lambda = 1$. The estimation method for $\langle L_{void} \rangle$ at $\lambda = 1$ is shown in the Supporting Information. **Fig.4(c)** shows the void stretching ratio, $\lambda_{void}$, as a function of global stretch ratio $\lambda$. The $\lambda_{void}$ of DN-2 gel is significantly larger than the affine deformation prediction. It increases nonlinearly with $\lambda$, particularly around $\lambda$ = 2.25–3.25, and decreases abruptly at yielding. In contrast, $\lambda_{void}$ of the DN-4 gel is slightly weaker than the affine deformation prediction. The extraordinary non-affine deformation of voids in the DN-2 gel indicates that deformation is highly

localized around the voids in DN-2 gel; however, it is not so in the DN-4 gel.

Next, the deformation of the nanometer-scale mesh of the first network was evaluated. The 1D parallel and perpendicular profiles in the high-$q$ region were fitted by the OZ functions and lengths $\xi$ were determined based on the mesh sizes of the first network in the two directions. The mesh deformation ratio of the first network, $\lambda_{mesh}$, was evaluated based on the mesh size at $\lambda = 1$. **Fig.4(d)** shows the local mesh deformation ratio of parallel ($\lambda_{mesh,p}$) and vertical ($\lambda_{mesh,v}$) directions as a function of the global stretch ratio $\lambda$ of the DN gels. For DN-2, $\lambda_{mesh,v}$ in the vertical direction almost follows the affine deformation until reaching necking, and a sudden decrease in $\lambda_{mesh,v}$ with yielding is observed. In contrast with $\lambda_{mesh,v}$, the deformation behavior, $\lambda_{mesh,p}$, in the parallel direction does not obey affine deformation. Before reaching the yielding point, $\lambda_{mesh,p}$ increased with the global $\lambda$; however, its value was significantly smaller than the affine deformation, and $\lambda_{mesh,p}$ also suddenly decreased at the yielding point. The $\lambda_{mesh,v}$ and $\lambda_{mesh,p}$ of the DN-4 gel were both smaller than the affine deformation, without showing sudden changes at the yielding point.

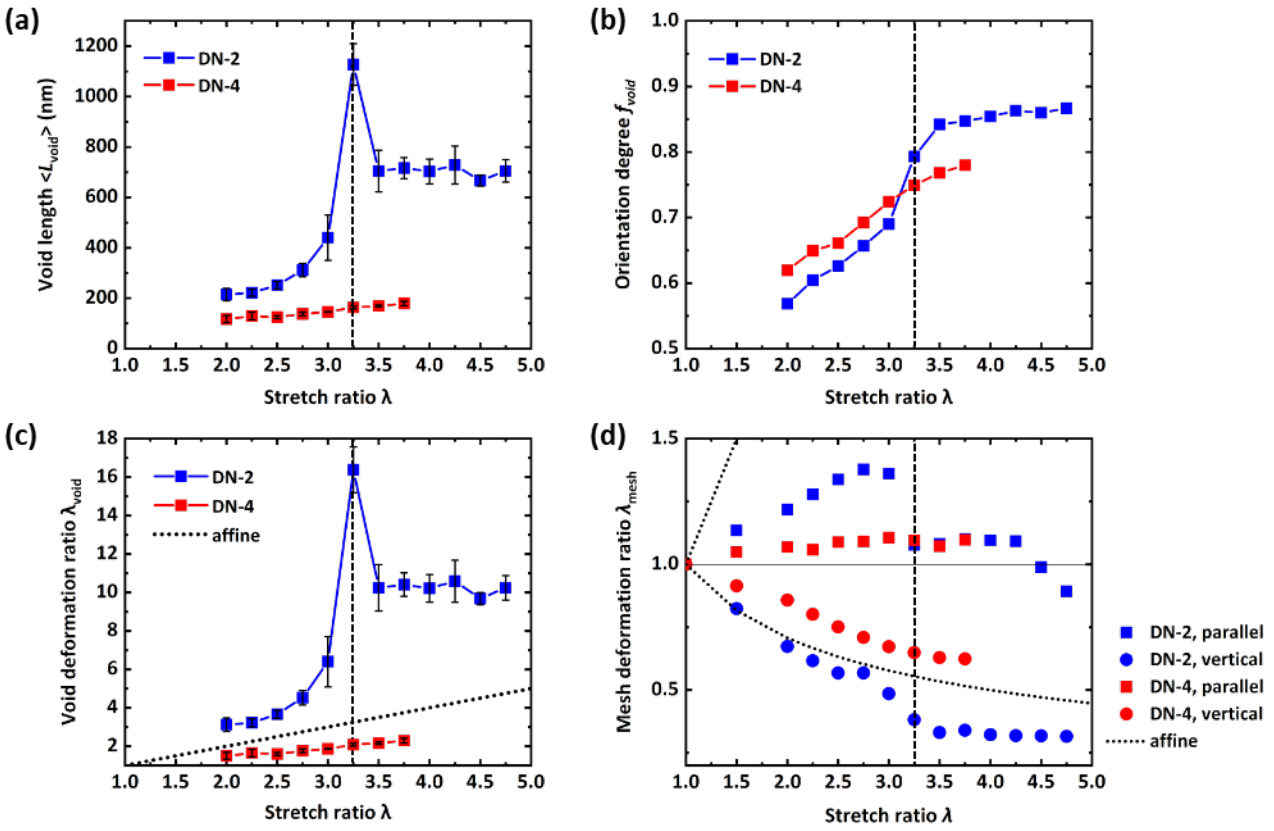


Fig.4 Structure evolution of the DN-2 and DN-4 samples as a function of global stretch ratio. The dashed line at λ=3.25 indicates the stretch ratio at the necking point for DN-2. (a) Long-axis length of voids. (b) Orientation degree of voids. (c) Void deformation ratio $\lambda_{void}$. (d) Mesh deformation ratio $\lambda_{mesh}$ of the first network. The dotted lines denote the affine deformation prediction. For DN-2 sample in necking regime, the results are obtained from the necked region.

Based on the nanometer-scale mesh deformation and submicrometer void deformation, we first discuss the structure of the DN-2 sample that shows necking. The sub-affine deformation of the mesh along the stretch direction indicates heterogeneous deformation of the samples and should be attributed to the internal fracturing of the first network. As shown by mechanical hysteresis, the internal fracturing of the first work starts to occur even at small $\lambda$ (~1.5), far below the yielding point.[20,22] Because the first network strands are in highly pre-stretched state by swelling ($\lambda_s$=4.14), the deformation capacity of the first network mesh in the DN gel is very small. So some of the first network strands start to rupture at very small stretch. As a result, the second network in the fractured first network region is largely stretched. The strain amplification in the fractured region largely compensates the less deformable mesh remaining in the first network to show a smaller mesh deformation ratio along the stretching direction than the affine deformation. Interestingly, $\lambda_{mesh,p}$ rapidly returns to the undeformed value at the necking point ($\lambda$ = 3.25) where necking starts to occur, which suggests that the first network was unloaded by the formation of the discontinuous structure (fragmentation) at the yield point. It implies that most of the stress in the DN-2 gel, after necking, is carried by the stretchable second network. Such observed local unloading of the first network is consistent with the fragmentation model of the first network proposed in previous studies.[2,19,25] From the large void deformation ratio along the stretch direction, $\lambda_{void}$, the fracturing in the first network

occurs from the pre-existing voids. Previous studies on swelling anisotropy indicate that selective fracturing of the first network propagates in the direction perpendicular to stretching.[19,26,38] Therefore, the fracturing in the first network occurs from lateral edges of voids because of stress concentration, along the direction vertical to the tensile deformation.

Next, we discuss the structure of the DN-4 sample. The sub-affine deformation of the voids as shown in **Figure 4(c)** indicates that the stretching-induced fracturing of the first network occurs homogeneously in the sample and is not localized around the voids even beyond the yielding point. This indicates that the internal fracturing process and mechanical behavior become less or even insensitive to voids, and the fracture occurs dispersedly over the entire sample, resulting in the yielding without necking. Because the second network at the fractured points of the first network deforms only modestly, we observe only small increase in the birefringence of the DN-4 as compared with its corresponding SN in **Figure 1(c)**. As shown in **Figure 4(d)**, the DN-4 showed less deformation of mesh both in the directions parallel with ($\lambda_{mesh,p}$) and vertical to ($\lambda_{mesh,v}$) the stretching, in comparison with those of the DN-2 gel. This could be attributed to the larger pre-stretch of the first network strands in the DN-4 gel ($\lambda_s$=4.72 for DN-4 vs $\lambda_s$=4.14 for DN-2) due to more larger swelling in the higher second monomer concentration.

**Fig.5** schematically illustrates the elucidated structural changes in uniaxially deformed DN gels

with different second network concentration. As shown in **Fig.5a**, the existence of first network void induces stress concentration around the void owing to differences in moduli between the non-void region where the modulus is dominated by the rigid first network and void region where only the soft second network exists. The fracturing process of the first network in DN gels depends on the modulus ($E$) and stretch ability ($\lambda_m$) differences between the first network ($E_1$ and $\lambda_{m,1}$) and the second network ($E_2$ and $\lambda_{m,2}$). For a fixed first network, the modulus ratio $E_1/E_2$ increases while stretch ability ratio $\lambda_{m,1}/\lambda_{m,2}$ decreases with the decrease of the second network concentration. At low second network concentration (DN-2), $E_1/E_2>>1$, so initial fracture in the first network occurs near the lateral edge of the voids by the stress concentration, and the fracture grows in the direction vertical to the stretch due to the relatively high stretching ability of the second network, which leads to anomalous void extension. On the other hand, at high second network concentration (DN-4), $E_1/E_2 \geq 1$, and the fracture also occurs near the lateral edge of the voids, similar to DN-2, but the stress concentration is largely suppressed, because the strain hardening of the second network occurs at relatively smaller stretching owing to its increase in the self-entanglement. As a result, the first network fracture also occurs in non-void region to show homogeneous fracture in the sample

As illustrated by the internal fracturing process of the DN gels in **Fig. 5b**, when tensile force is

applied to the DN gels with relatively low second monomer concentration ($E_1 >> E_2$), the pre-stretched first network strands are selectively fractured near the lateral edges of voids, which induces remarkable stretching of the soft second network to carry the load, as seen by the significantly stronger birefringence in comparison with its corresponding SN gel in **Figure 1(c)**. The local strain amplification by fracturing of the first network makes the voids deform more than the affine deformation. With the progress of stretching, such regioselective internal fracturing of voids induces percolation of the fracture in the lateral direction, resulting in the necking behavior and unloading of the first network. At an elevated second monomer concentration ($E_1 \geq E_2$), the modulus of the second network increases and the stretching ability decreases owing to its increase in the self-entanglement, resulting in the suppression of the stress concentration near the voids.

The proposed internal fracturing scenario in **Fig.5** suggests that the key reason for the necking of DN gels is the sufficiently large contrasts in moduli and extensibilities between the two networks, which induces significant strain amplification around the voids (or defects). Even for the relatively homogeneous first network not containing the submicrometer-scale voids, necking should also occur when the stress concentration is sufficiently strong. As seen in the DN gels with the tetra-PEG first network that does not contain large-scale spatial inhomogeneity, necking occurs when the second network is relatively soft.[24,49]

This is because there should be small-scale defects even in the tetra-PEG network, which can induce local strain amplification near the defects and lead to propagation of first network fracture to show necking.

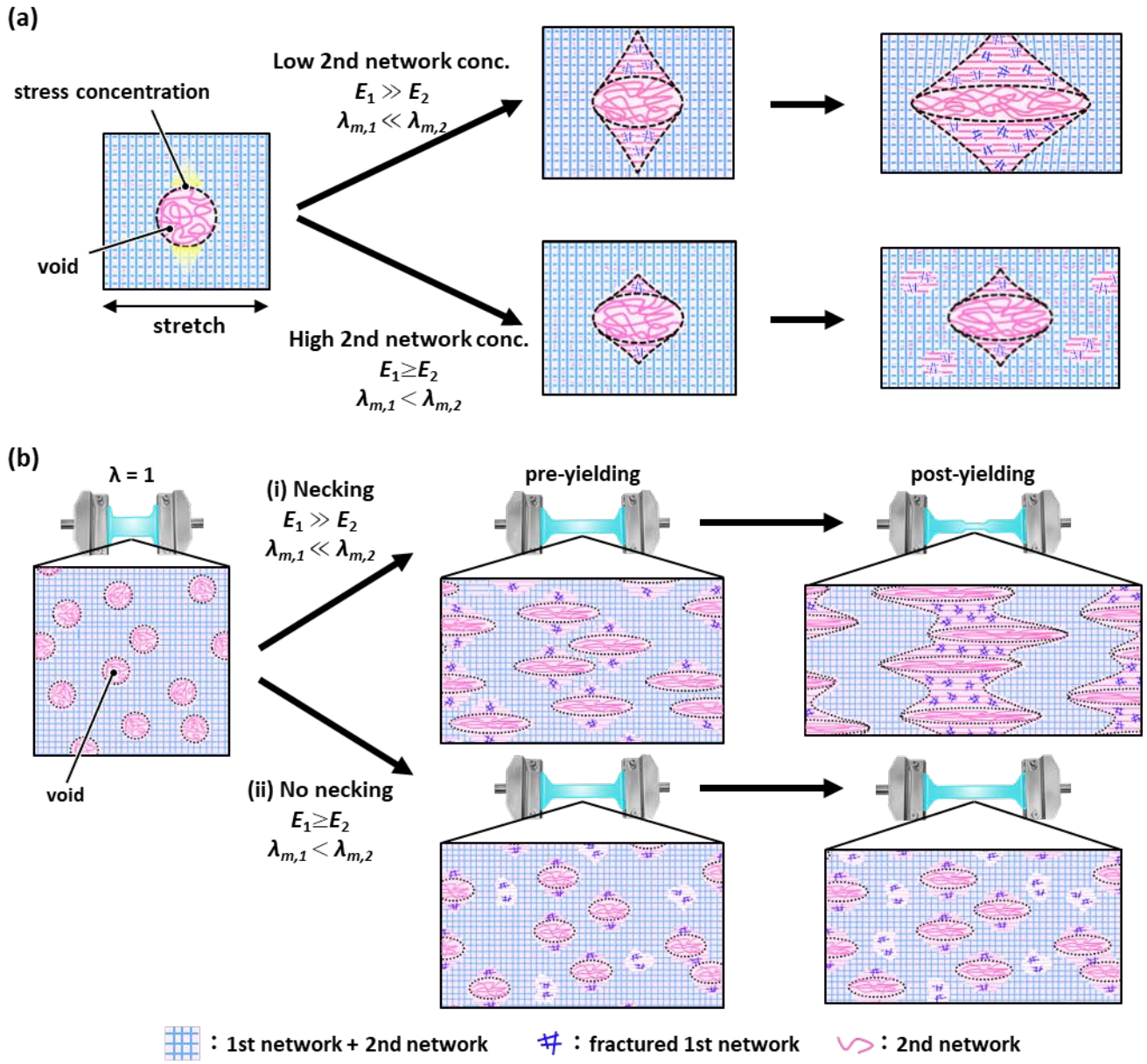


Fig.5 Schematic illustration of fracturing process of the first network in DN gels with different second network concentration. (a) Stress concentration and first network fracture around the void (defect) depend on the difference in modulus ($E$) and stretch ability ($\lambda_m$) between the first ($E_1$ and $\lambda_{m,1}$) and second ($E_2$ and $\lambda_{m,2}$) networks, respectively. For a constant structure of the first network, the ratio $E_1/E_2$ and $\lambda_{m,2}/\lambda_{m,1}$ increases with the decrease of second network concentration. DN gel with low second network concentration has a strong stress concentration around the lateral edge of void to cause fracture with large crack opening of the first network in the direction vertical to the stretch, while the DN gel with high second network concentration has weak stress concentration and small crack opening around the void, so the first network fracture occurs also in non-void region. (b) DN gel with strong stress concentration causes necking behavior (i) and DN gel with weak stress concentration does not (ii) under uniaxial tensile process. When $E_1/E_2 >> 1$, the fracture of first network, starting from the lateral edge of the voids, propagates and percolates in the direction vertical to the tensile deformation, resulting the necking behavior of the DN gels. Such fracture process leads to anomalous void extension. When $E_1/E_2 \geq \mathbf{1}$, the stress concentration near the voids is suppressed and the first network fractures dispersedly over the sample even at post-yielding region, showing no necking.

## Conclusions

We investigated structural changes in DN gels under uniaxial stretching, both in nanometer- and submicrometer-scale by SAXS measurements. We found that the mechanical balance between the two networks determines the internal fracturing process in DN gels. For the DN-2 gel with significant differences in moduli and stretch abilities between the two networks, internal fracturing is initiated near the voids in the lateral direction and propagated along the direction vertical to the stretching; and percolation of the fracture in lateral direction triggers necking of the sample. For the DN-4 gel with relatively less differences in moduli and stretch abilities between the two networks, internal fracturing occurs dispersedly over the sample, irrespective of the presence of voids. This study deepens the understanding on the toughening and yielding mechanisms of DN systems, which is useful for designing DN gels with desired mechanical properties for various applications.

## Acknowledgements

This research was supported by JSPS KAKENHI grant numbers JP17H06144 and JP26820300. This research was also partially funded by ImPACT Program of Council for Science, Technology and Innovation (Cabinet Office, Government of Japan). Institute for Chemical Reaction Design and Discovery

(ICReDD) was established by World Premier International Research Initiative (WPI), MEXT, Japan. The authors thank Dr. Taiki Hoshino, Dr. So Fujinami, and Dr. Tomotaka Nakatani (RIKEN, Japan) for their kind assistance with the SAXS measurement at SPring-8. K. Fukao acknowledges Hokkaido University's "Ambitious Leader's Program" supported by MEXT, Japan. The authors thank R. Kiyama and T. Matsuda for their kind advice during this research. The authors thank Prof. Herbert Hui for suggestive discussion on the stress concentration.

**Supporting Information Available**: This material is available free of charge via the Internet at http://pubs.acs.org.

additional experimental section (SAXS measurement and indentation test), comparison of the mesh size obtained from SAXS and from mechanical test, Ruland plot analysis, summary of sample properties (PDF)

## References

(1) Gong, J. P.; Katsuyama, Y.; Kurokawa, T.; Osada, Y. Double-Network Hydrogels with Extremely High Mechanical Strength. *Advanced Materials* **2003**, *15* (14), 1155–1158.

(2) Gong, J. P. Why Are Double Network Hydrogels so Tough? *Soft Matter* **2010**, *6* (12), 2583–2590.

(3) Sun, J. Y.; Zhao, X.; Illeperuma, W. R. K.; Chaudhuri, O.; Oh, K. H.; Mooney, D. J.; Vlassak, J. J.; Suo, Z. Highly Stretchable and Tough Hydrogels. *Nature* **2012**, *489* (7414), 133–136.

(4) Myung, D.; Waters, D.; Wiseman, M.; Duhamei, P. E.; Noolandi, J.; Ta, C. N.; Frank, C. W. Progress in the Development of Interpenetrating Polymer Network Hydrogels. *Polymers for Advanced Technologies* **2008**, *19* (6), 647–657.

(5) Ducrot, E.; Chen, Y.; Bulters, M.; Sijbesma, R. P.; Creton, C. Toughening Elastomers with Sacrificial Bonds and Watching Them Break. *Science* **2014**, *344* (6180), 186–189.

(6) Matsuda, T.; Nakajima, T.; Gong, J. P. Fabrication of Tough and Stretchable Hybrid Double-Network Elastomers Using Ionic Dissociation of Polyelectrolyte in Nonaqueous Media. *Chemistry of Materials* **2019**, *31*, 3766–3776.

(7) Saito, J.; Furukawa, H.; Kurokawa, T.; Kuwabara, R.; Kuroda, S.; Hu, J.; Tanaka, Y.; Gong, J. P.; Kitamura, N.; Yasuda, K. Robust Bonding and One-Step Facile Synthesis of Tough Hydrogels with Desirable Shape by Virtue of the Double Network Structure. *Polymer Chemistry* **2011**, *2* (3), 575–580.

(8) Chen, Q.; Zhu, L.; Zhao, C.; Wang, Q.; Zheng, J. A Robust, One-Pot Synthesis of Highly Mechanical and Recoverable Double Network Hydrogels Using Thermoreversible Sol-Gel

Polysaccharide. *Advanced Materials* **2013**, *25* (30), 4171–4176.

(9) Argun, A.; Can, V.; Altun, U.; Okay, O. Nonionic Double and Triple Network Hydrogels of High Mechanical Strength. *Macromolecules* **2014**, *47* (18), 6430–6440.

(10) Feng, X.; Ma, Z.; MacArthur, J. V.; Giuffre, C. J.; Bastawros, A. F.; Hong, W. A Highly Stretchable Double-Network Composite. *Soft Matter* **2016**, *12* (44), 8999–9006.

(11) Takahashi, R.; Sun, T. L.; Saruwatari, Y.; Kurokawa, T.; King, D. R.; Gong, J. P. Creating Stiff, Tough, and Functional Hydrogel Composites with Low-Melting-Point Alloys. *Advanced Materials* **2018**, *30* (16), 1–7.

(12) Nakajima, T.; Sato, H.; Zhao, Y.; Kawahara, S.; Kurokawa, T.; Sugahara, K.; Gong, J. P. A Universal Molecular Stent Method to Toughen Any Hydrogels Based on Double Network Concept. *Advanced Functional Materials* **2012**, *22* (21), 4426–4432.

(13) Yasuda, K.; Kitamura, N.; Gong, J. P.; Arakaki, K.; Kwon, H. J.; Onodera, S.; Chen, Y. M.; Kurokawa, T.; Kanaya, F.; Ohmiya, Y.; et al. A Novel Double-Network Hydrogel Induces Spontaneous Articular Cartilage Regeneration in Vivo in a Large Osteochondral Defect. *Macromolecular Bioscience* **2009**, *9* (4), 307–316.

(14) Nonoyama, T.; Wada, S.; Kiyama, R.; Kitamura, N.; Mredha, M. T. I.; Zhang, X.; Kurokawa, T.;

Nakajima, T.; Takagi, Y.; Yasuda, K.; et al. Double-Network Hydrogels Strongly Bondable to Bones by Spontaneous Osteogenesis Penetration. *Advanced materials* **2016**, *28* (31), 6740–6745.

(15) Matsuda, T.; Kawakami, R.; Namba, R.; Nakajima, T.; Gong, J. P. Mechanoresponsive Self-Growing Hydrogels Inspired by Muscle Training. *Science* **2019**, *363* (6426), 504–508.

(16) Naficy, S.; Razal, J. M.; Whitten, P. G.; Wallace, G. G.; Spinks, G. M. A PH-Sensitive, Strong Double-Network Hydrogel: Poly(Ethylene Glycol) Methyl Ether Methacrylates-Poly(Acrylic Acid). *Journal of Polymer Science, Part B: Polymer Physics* **2012**, *50* (6), 423–430.

(17) Chen, Q.; Chen, H.; Zhu, L.; Zheng, J. Engineering of Tough Double Network Hydrogels. *Macromolecular Chemistry and Physics* **2016**, *217* (9), 1022–1036.

(18) Sun, T. L.; Kurokawa, T.; Kuroda, S.; Ihsan, A. Bin; Akasaki, T.; Sato, K.; Haque, M. A.; Nakajima, T.; Gong, J. P. Physical Hydrogels Composed of Polyampholytes Demonstrate High Toughness and Viscoelasticity. *Nature materials* **2013**, *12* (10), 932–937.

(19) Nakajima, T.; Kurokawa, T.; Ahmed, S.; Wu, W. L.; Gong, J. P. Characterization of Internal Fracture Process of Double Network Hydrogels under Uniaxial Elongation. *Soft Matter* **2013**, *9* (6), 1955–1966.

(20) Webber, R. E.; Creton, C.; Brown, H. R.; Gong, J. P. Large Strain Hysteresis and Mullins Effect

of Tough Double-Network Hydrogels. *Macromolecules* **2007**, *40* (8), 2919–2927.

(21) Mai, T. T.; Matsuda, T.; Nakajima, T.; Gong, J. P.; Urayama, K. Distinctive Characteristics of Internal Fracture in Tough Double Network Hydrogels Revealed by Various Modes of Stretching. *Macromolecules* **2018**, *51* (14), 5245–5257.

(22) Mai, T. T.; Matsuda, T.; Nakajima, T.; Gong, J. P.; Urayama, K. Damage Cross-Effect and Anisotropy in Tough Double Network Hydrogels Revealed by Biaxial Stretching. *Soft Matter* **2019**, *15* (18), 3719–3722.

(23) Ahmed, S.; Nakajima, T.; Kurokawa, T.; Anamul Haque, M.; Gong, J. P. Brittle-Ductile Transition of Double Network Hydrogels: Mechanical Balance of Two Networks as the Key Factor. *Polymer* **2014**, *55* (3), 914–923.

(24) Matsuda, T.; Nakajima, T.; Fukuda, Y.; Hong, W.; Sakai, T.; Kurokawa, T.; Chung, U. Il; Gong, J. P. Yielding Criteria of Double Network Hydrogels. *Macromolecules* **2016**, *49* (5), 1865–1872.

(25) Na, Y.-H.; Tanaka, Y.; Kawauchi, Y.; Furukawa, H.; Sumiyoshi, T.; Gong, J. P.; Osada, Y. Necking Phenomenon of Double-Network Gels. *Macromolecules* **2006**, *39* (14), 4641–4645.

(26) Guo, H.; Hong, W.; Kurokawa, T.; Matsuda, T.; Wu, Z. L.; Nakajima, T.; Takahata, M.; Sun, T.; Rao, P.; Gong, J. P. Internal Damage Evolution in Double-Network Hydrogels Studied by

Microelectrode Technique. *Macromolecules* **2019**, *52*, 7114–7122.

(27) Bastide, J.; Leibler, L. Large-Scale Heterogeneities in Randomly Cross-Linked Networks. *Macromolecules* **1988**, *21* (8), 2647–2649.

(28) Hiroi, T.; Kondo, S.; Sakai, T.; Gilbert, E. P.; Han, Y. S.; Kim, T. H.; Shibayama, M. Fabrication and Structural Characterization of Module-Assembled Amphiphilic Conetwork Gels. *Macromolecules* **2016**, *49* (13), 4940–4947.

(29) Na, Y. H.; Kurokawa, T.; Katsuyama, Y.; Tsukeshiba, H.; Gong, J. P.; Osada, Y.; Okabe, S.; Karino, T.; Shibayama, M. Structural Characteristics of Double Network Gels with Extremely High Mechanical Strength. *Macromolecules* **2004**, *37* (14), 5370–5374.

(30) Huang, M.; Furukawa, H.; Tanaka, Y.; Nakajima, T.; Osada, Y.; Gong, J. P. Importance of Entanglement between First and Second Components in High-Strength Double Network Gels. *Macromolecules* **2007**, *40* (18), 6658–6664.

(31) Furukawa, H.; Kuwabara, R.; Tanaka, Y.; Kurokawa, T.; Na, Y. H.; Osada, Y.; Gong, J. P. Tear Velocity Dependence of High-Strength Double Network Gels in Comparison with Fast and Slow Relaxation Modes Observed by Scanning Microscopic Light Scattering. *Macromolecules* **2008**, *41* (19), 7173–7178.

(32) Tominaga, T.; Tirumala, V. R.; Lin, E. K.; Gong, J. P.; Furukawa, H.; Osada, Y.; Wu, W. li. The Molecular Origin of Enhanced Toughness in Double-Network Hydrogels: A Neutron Scattering Study. *Polymer* **2007**, *48* (26), 7449–7454.

(33) Tominaga, T.; Tirumala, V. R.; Lee, S.; Lin, E. K.; Gong, J. P.; Wu, W. L. Thermodynamic Interactions in Double-Network Hydrogels. *Journal of Physical Chemistry B* **2008**, *112* (13), 3903–3909.

(34) Tirumala, V. R.; Tominaga, T.; Lee, S.; Butler, P. D.; Lin, E. K.; Gong, J. P.; Wu, W. L. Molecular Model for Toughening in Double-Network Hydrogels. *Journal of Physical Chemistry B* **2008**, *112* (27), 8024–8031.

(35) Tsukeshiba, H.; Huang, M.; Na, Y. H.; Kurokawa, T.; Kuwabara, R.; Tanaka, Y.; Furukawa, H.; Osada, Y.; Gong, J. P. Effect of Polymer Entanglement on the Toughening of Double Network Hydrogels. *Journal of Physical Chemistry B* **2005**, *109* (34), 16304–16309.

(36) Nakajima, T.; Furukawa, H.; Tanaka, Y.; Kurokawa, T.; Gong, J. P. Effect of Void Structure on the Toughness of Double Network Hydrogels. *Journal of Polymer Science, Part B: Polymer Physics* **2011**, *49* (17), 1246–1254.

(37) Ducrot, E.; Montes, H.; Creton, C. Structure of Tough Multiple Network Elastomers by Small

Angle Neutron Scattering. *Macromolecules* **2015**, *48* (21), 7945–7952.

(38) Fukao, K.; Nonoyama, T.; Kiyama, R.; Furusawa, K.; Kurokawa, T.; Nakajima, T.; Gong, J. P. Anisotropic Growth of Hydroxyapatite in Stretched Double Network Hydrogel. *ACS Nano* **2017**, *11* (12), 12103–12110.

(39) Shibayama, M. Spatial Inhomogeneity and Dynamic Fluctuations of Polymer Gels. *Macromolecular Chemistry and Physics*. 1998, pp 1–30.

(40) Chalal, M.; Ehrburger-Dolle, F.; Morfin, I.; Bley, F.; Aguilar De Armas, M. R.; López Donaire, M. L.; San Roman, J.; Bölgen, N.; Pişkin, E.; Ziane, O.; et al. SAXS Investigation of the Effect of Temperature on the Multiscale Structure of a Macroporous Poly(N-Isopropylacrylamide) Gel. *Macromolecules* **2010**, *43* (4), 2009–2017.

(41) Ryu, J.; Ko, J.; Lee, H.; Shin, T. G.; Sohn, D. Structural Response of Imogolite-Poly(Acrylic Acid) Hydrogel under Deformation. *Macromolecules* **2016**, *49* (5), 1873–1881.

(42) Jaspers, M.; Pape, A. C. H.; Voets, I. K.; Rowan, A. E.; Portale, G.; Kouwer, P. H. J. Bundle Formation in Biomimetic Hydrogels. *Biomacromolecules* **2016**, *17* (8), 2642–2649.

(43) Salamon, K.; Aumiler, D.; Pabst, G.; Vuletić, T. Probing the Mesh Formed by the Semirigid Polyelectrolytes. *Macromolecules* **2013**, *46* (3), 1107–1118.

(44) Marciel, A. B.; Srivastava, S.; Tirrell, M. V. Structure and Rheology of Polyelectrolyte Complex Coacervates. *Soft Matter* **2018**, *14* (13), 2454–2464.

(45) Thünemann, A. F.; Ruland, W. Microvoids in Polyacrylonitrile Fibers: A Small-Angle X-Ray Scattering Study. *Macromolecules* **2000**, *33* (5), 1848–1852.

(46) Keum, J. K.; Zuo, F.; Hsiao, B. S. Formation and Stability of Shear-Induced Shish-Kebab Structure in Highly Entangled Melts of UHMWPE/HDPE Blends. *Macromolecules* **2008**, *41* (13), 4766–4776.

(47) Cui, K.; Meng, L.; Tian, N.; Zhou, W.; Liu, Y.; Wang, Z.; He, J.; Li, L. Self-Acceleration of Nucleation and Formation of Shish in Extension-Induced Crystallization with Strain beyond Fracture. *Macromolecules* **2012**, *45* (13), 5477–5486.

(48) Kawai, T.; Soeno, S.; Kuroda, S. ichi; Koido, S.; Nemoto, T.; Tamada, M. Deformation Induced Void Formation and Growth in β Nucleated Isotactic Polypropylene. *Polymer* **2019**, *178* (June), 121523.

(49) Nakajima, T.; Fukuda, Y.; Kurokawa, T.; Sakai, T.; Chung, U. Il; Gong, J. P. Synthesis and Fracture Process Analysis of Double Network Hydrogels with a Well-Defined First Network. *ACS Macro Letters* **2013**, *2* (6), 518–521.